scientific reports

Check for updates

OPEN

Deferential nephrotoxicity effect of lanthanum oxide nanoparticle responses to concentration and time in *vivo*

Nouf M. Alyami[1,4]✉, Ghufran A. Almuhaini[1,4], Hussah Alobaid[1], Saleh Maodaa[1], Noura M. Alshiban[2], Zainab Ali Alnakhli[1], Faten Jamal Alashkar[1], Khalid Elfaki Ibrahim[1], Saeed Alqahtani[2], Rafa Almeer[1], Hanadi M. Alyami[3] & Saud Alarifi[1]

Lanthanum oxide nanoparticles (La_2O_3 NPs) possess unique electronic properties. The increased use of La_2O_3 NPs raises the risk of exposure, potentially leading to bioaccumulation and metabolic disruptions. This study examines the impact of La_2O_3 NPs on the kidneys of mice administered intraperitoneally (i.p) at doses of 60, 150, and 300 mg/kg for 14 and 35 days. Results indicated variations in *SOD* gene expression and GSH plasma levels that were inversely correlated with NP dosage. A strong positive relationship was found between the inflammatory marker NOS2 transcription and NP dose, confirming pro-inflammatory effects based on concentration. Significant elevations, particularly at lower NP doses, were observed with *KIM-1*, uric acid, urea, ALP, ALT, and AST, indicating kidney and liver dysfunction. Furthermore, markers of kidney inflammation, as determined by protein array, intensified with prolonged exposure to the lowest concentrations of La_2O_3 NPs. In contrast, higher doses initially caused inflammation that subsided over time. Along with the disruption of mineral balance detected by Inductively Coupled Plasma Mass spectrometry (ICP-MS) (specifically the loss of Ca^{2+}), we believe these factors are the main contributors to nephrotoxicity, the adverse effects of La_2O_3 NPs releasing free La^{3+} ions, which mimic calcium-activating ROS production that worsens at lower concentrations due to their reduced aggregation and enhanced ability to penetrate the cell membrane. However, further studies must confirm whether these effects result from direct nanoparticle circulation in the bloodstream or secondary toxicity mechanisms.

Keywords Lanthanum oxide, Nanoparticle, ROS, Toxicity, Inflammation, Kidney injury, Cytokines, Rare Earth elements, ICP-MS, Protein array

Nanoparticles, with sizes ranging from 1 to 100 nm, are widely utilized across diverse industries, including pharmaceuticals, agriculture, and food processing. Their integration into daily life has brought benefits and challenges, particularly concerning human health[1–3]. Nanoparticles derived from rare earth elements (REEs) have recently gained attention for their catalytic, energy, and theranostics applications[4]. However, these elements pose environmental risks, entering ecosystems through mining and smelting activities[4]. As REEs, lanthanum oxide (La_2O_3) is valued for its unique electronic configurations and is used in energy-saving materials, fluorescent lamps, glass manufacturing, and micro-fertilizers. Despite its utility, the release of trivalent lanthanum ions (La^{3+}) from agricultural applications can contaminate water sources. This can lead to bioaccumulation in the food chain and interfere with metabolic processes, as these NPs can penetrate cellular membranes and generate reactive oxygen species (ROS)[5]. La_2O_3 NPs raise serious concerns regarding their toxicological impact on human health and ecological systems. Among the organs at risk, the kidneys play a critical role in detoxifying and excreting xenobiotics, making them highly susceptible to nanoparticle-induced toxicity[6,7].

This interaction disrupts the oxidative balance, inducing apoptosis and inflammation in various tissues in *vivo* exposed for 30 or 60 days, whether through inhalation or oral ingestion. Additionally, it has been confirmed that

[1]Department of Zoology, College of Science, King Saud University, P.O. Box 2455, Riyadh 11451, Saudi Arabia. [2]Advanced Diagnostics and Therapeutics Institute, King Abdulaziz City for Science and Technology (KACST), Health Sector, Riyadh 11442, Saudi Arabia. [3]Specialized Dentistry Department, King Fahad Medical City, Riyadh Second Health Cluster, Riyadh 11451, Saudi Arabia. [4]Nouf M. Alyami and Ghufran A. Almuhaini contributed equally. ✉email: nalyami@ksu.edu.sa

a single i.p. induction can trigger these features after one week[8–12]. The kidneys have highly specialized structures, including the glomerulus and tubular epithelium, which may be exposed to lanthanum oxide nanoparticles through filtration and systemic circulation. This exposure poses a significant threat to the nephron—the functional unit of the kidney—potentially disrupting essential physiological processes such as glomerular filtration, tubular reabsorption, and secretion[7]. Research indicates that lanthanum accumulates elevated in the liver, lungs, and kidneys as renal impairment progresses. This is particularly concerning as lanthanum-based compounds, including phosphate binders, are commonly used in the treatment of hyperphosphatemia in patients with chronic kidney disease (CKD)[13–15].

Despite increasing evidence of La_2O_3 NPs toxicity, significant gaps in knowledge remain. Most studies have focused on acute toxicity at high doses, while the effects of chronic, low-dose exposure are not well understood. Additionally, the interactions of La_2O_3 NPs with nephron structures, such as proximal tubules and the loop of Henle, require further investigation. A key question is whether nephrotoxic effects result from the physical interaction of the nanoparticles or the free ions released during degradation. This study addresses these issues by examining the nephrotoxic effects of La_2O_3 NPs, focusing on the roles of oxidative stress and inflammation in kidney injury and emphasizing dose- and time-dependent toxicity mechanisms.

Method and materials

Experimental animal preparation

Forty-two female albino Swiss mice (Mus musculus) were obtained from the animal house of the Zoology Department at King Saud University in Riyadh, Saudi Arabia. The mice had an average weight of 25 to 30 g and were housed at the same facility throughout the experiment. They were individually kept in ventilated cage (IVC) racks within a controlled environment, with a temperature of 22 ± 2 °C and humidity of 55 ± 5%, and a 12-hour light/12-hour dark cycle, and given unrestricted access to food and water. This investigation was carried out in compliance with the ARRIVE criteria for reporting research involving animals, guaranteeing comprehensive documentation of the experimental design, techniques, and results. The Institutional Animal Care and Use Committee (IACUC) of King Saud University granted approval for the experimental protocol. (Ref. No.: KSU-SE-22-75). Notably, all procedures involving animals were conducted in accordance with relevant guidelines and regulations, ensuring compliance with ethical standards for the care and use of laboratory animals.

Experimental animals and la_2o_3 nanoparticle induction

After a week of acclimatization, the mice were randomly assigned to seven groups ($n = 6$). According to the OECD 401 reports, the lethal dose (LD50) of La_2O_3 NPs administered orally to rats exceeds 12 g/kg body weight[5,14]. The NPs were prepared in Milli-Q water at three concentrations (60, 150, and 300 mg/kg), sonicated at 100 W on ice for 10 min, and then administered only once via i.p., as described in Alyami et al. (2024)[12]. Utilizing i.p. induction guarantees precise nanoparticle concentration and quantity. Our earlier research shows that administering a single i.p. dose of nanoparticles produces ROS that negatively affects the mice's liver after one week at 60, 150, and 300 mg/kg doses[12]. However, in this investigation, we further extend the duration of 14 and 35 days and monitor the kidney function. The groups were divided as follows:

Group 1 Control group, receiving Milli-Q water i.p.

Group 2 60 mg/kg La_2O_3 NPs i.p. for 14 days.

Group 3 60 mg/kg La_2O_3 NPs i.p. for 35 days.

Group 4 150 mg/kg La_2O_3 NPs i.p. for 14 days.

Group 5 150 mg/kg La_2O_3 NPs i.p. for 35 days.

Group 6 300 mg/kg La_2O_3 NPs i.p. for 14 days.

Group 7 300 mg/kg La_2O_3 NPs i.p. for 35 days.

Characterization of la_2o_3 NPs

The La_2O_3 NPs were obtained from US Research Nanomaterials, Inc., Houston, TX (La_2O_3, 99.99%, 10–100 nm), Stock No. US3265, CAS No. 1312-81-8. They were characterized using a scanning electron/transmission microscope (SEM/TEM) and Energy-dispersive X-ray spectroscopy (EDS) (JSM-IT500HR SEM, Jeol Inc., Peabody, MA, USA), operated at 1 m 10.0 kV, coupled with OriginPro 2021 (OriginLab Corporation, Northampton, MA, USA). X-ray diffraction (XRD) (Rigaku, Tokyo, Japan) operated at 9 kW. The Rigaku Miniflex 300/600 (Tokyo, Japan) with Cu Kα radiation (λ = 1.5148 Å) utilized a voltage of 40 kV and a current of 15 mA to evaluate the crystallinity and amorphous structure of the samples and scanned between 3° and 60° diffraction angles (2θ) at 5°/min. Additionally, Fourier-Transform Infrared Spectroscopy (FTIR) was performed using a Thermo Smart ATR IS20 Spectrometer (Thermo Fisher Scientific, Waltham, MA, USA) at a wavenumber range of 4000 –600 cm – 1, with 32 scans and a resolution of 4 cm – 1. Finally, to measure the Brunauer–Emmett–Teller (BET) surface areas, nitrogen adsorption-desorption was conducted by flowing liquid nitrogen at 77 K (– 196 °C) using the Micromeritics ASAP 2020 Physisorption analyzer.

Blood collection and tissue preparation

After 14 or 35 days, blood samples were obtained from the mice under ketamine/xylazine anesthesia, with doses of 90 mg/kg and 10 mg/kg, respectively, based on the mice's weight. The blood sample was allowed to clot at room temperature and centrifuged for 15 min at 3000 rpm. Serum aliquots for biochemical examination were collected and frozen at -20 °C. The Liver and kidney were extracted from each animal, divided into potions, and kept at -80 °C for analysis. For histological examination, a portion was preserved in 10% neutral buffered formalin for one week, then rinsed, embedded in paraffin wax, sectioned at 7 µm, stained with hematoxylin and eosin (H&E), and examined under a light microscope using Mayer's modified staining method.

Enzymatic analysis

Following the collection of mouse serum, we utilized it to quantify the activity of enzymes, namely Alkaline phosphatase (ALP), Alanine transaminase (ALT), Aspartate aminotransferase (AST), and Glutathione (GSH), following the procedures outlined in Pratt and Kaplan[16]. Additionally, we analyzed kidney enzymes, uric acid, and urea per the manufacturer's kit protocol from Bioanalyzed.

RNA extraction

Total Ribonucleic acid (RNA) was extracted from 30 mg of kidney tissue after washing it three times with a cold phosphate-buffered saline (PBS) solution. The tissue was then homogenized on ice using a glass homogenizer and 0.7 ml of TRIzol™ Reagent (Catalog No. 15596026, Thermo Fisher), following the manufacturer's instructions. Using the NanoDrop ND-1000 (Thermo Fisher), RNA purity and concentration were determined, with a ratio of ~ 2 considered indicative of purity. The samples were stored in a -80 °C freezer.

Reverse transcription-quantitative PCR (RT-qPCR)

To synthesize complementary DNA (cDNA), we used 1 µg of total RNA and followed the manufacturer's instructions for this step. We used the OneScript® Hot cDNA Synthesis Kit (Catalog No. G594, abm) for the synthesis. Reverse transcription-quantitative PCR (RT-qPCR) was performed using HOT FIREPol EvaGreen qPCR Mix Plus (ROX) from Solis Biodyne (Catalog No. 08-24-00001). The final reaction volume was 25 µL, containing 50 ng of cDNA and 250 nM of each forward and reverse primer. The real-time PCR Detection System was from Bio-Rad, USA, with a denaturation temperature of 95 °C for 15 s (sec), an annealing of 60 °C for 20 s, and an extension of 72 for 20 s, repeated 40 times. Gene expression analysis employed the $2^{-\Delta\Delta Ct}$ method, normalized to *Polr2a* as a housekeeping gene, as explained in the references[17]. In this study, we targeted the following genes listed in Table 1. The primers were selected from the pre-review paper and confirmed using the National Center for Biotechnology Information (NCBI) Primer-BLAST tool, with the final product size visualized in 2% agarose gel.

Mouse cytokines signaling array

In our study on the impact of La_2O_3 nanoparticles on mouse kidneys, we followed the manufacturer's instructions and used a 2 mg/mL array from RayBio®, called the Cytokine Antibody Arrays - Mouse Cytokine Antibody Array System 3. Kidney lysates from the 60 mg/kg and 300 mg/kg groups were used in this experiment, which showed the most histopathological damage. The total protein was quantified using a BSA Protein Assay and loaded at 2 mg/ml for each sample. The array detects 38 antibodies that regulate apoptosis, inflammation, and immune response. The results were visualized using chemiluminescence detection with ChemiDoc and then analyzed using Image Lab software (RRID: SCR_014210). The quantified pixels were normalized using a specific algorithm using RayBio® Excel to ensure the accuracy of our data. Finally, the data was presented as fold change ratios (log^{10}) relative to the untreated control.

Inductively coupled plasma mass spectrometry (ICP-MS)

The mineral content in kidney tissue was analyzed using a NexION 300X ICP-MS (PerkinElmer, Inc.). For every 0.5 gram of tissue, we added 2 mL of deionized water (dH2o) and 5 ml of 65% nitric acid (HNO3) (Sigma-Aldrich), optimized based on the tissue weights. We boiled the mixture at 235 °C until all the tissue was digested and formed an ash structure. Then, the samples were washed three times using 5 mL of dH2O through filter paper. A filtered 15 mL solution was collected, and 5 mL of 1% HNO3 was added. The samples were stored at 4 °C until loaded into the ICP-MS and ran with the standards. Stock solutions of the individual and multi-element standards were prepared (1,000.0 µg/mL, ULTRA Scientific) and further diluted with nitric

Gene name	Sequences	Size	References
RNA polymerase II subunit A (Polr2a)	5′-ATCAACAATCAGCTGCGGCG-3′ 5′-GCCAGACTTCTGCATGGCAC-3′	144 bp	[18]
Superoxide dismutase (SOD)	5′-GGAACCATCCACTTCGAGCA-3′ 5′-CGTCCTTTCCAGCAGTCACA-3′	232 bp	[19]
Kidney injury molecule 1 (KIM-1)	5′-ACATATCGTGGAATCACAACGAC-3′ 5′-ACAAGCAGAAGATGGGCATTG-3′	60 bp	[19]
Nitric oxide synthase 2, inducible (Nos2)	5′-ACTACTGCTGGTGGTGACAA-3′ 5′-CCTGAAGGTGTGGTTGAGTTC-3′	109 bp	[20]

Table 1. RT-qPCR primer sequences, product size, and references paper.

acid to obtain the desired range of dilutions (1:10). The quality control and the limits of detection (LOD) were performed as mentioned and published by Brima et al., 2016[21].

Statistical analysis

Statistical significance was assessed using a one-way analysis of variance (ANOVA) followed by Dunnett post-hoc test, with a p-value of ≤ 0.05 considered statistically significant. Results are presented as mean ± standard error of the mean (SEM) or standard deviation (SD) using GraphPad Prism 9.

Results

Chemical composition study for the la_2o_3 NPs

X-ray spectroscopy (EDS) analysis

EDS analysis of the nanoparticle samples indicates the presence of elements such as lanthanum, oxygen, chlorine, aluminum, and platinum (Fig. 1a). The nanoparticles were collected on aluminum foil and treated with chlorine to remove insulating surface layers, including hydroxides and carbonates, and to improve the adhesion of the 2 nm platinum coating layer. This was achieved using a JEC-3000FC auto fine coater (JEOL Inc., Peabody, MA, USA), which enhanced conductivity and imaging quality. Lanthanum (La) comprises the highest weight% in the sample, accompanied by a notable quantity of oxygen (O) and a small amount of chlorine (Cl), aluminum (Al), and platinum (Pt), as detailed in Fig. 2. The weight percentages (wt%) for the La_2O_3 nanoparticle nanoparticles are recorded as La 80.4% and O 14.2%, aligning with earlier findings[22].

Fourier-transform infrared spectroscopy analysis

FTIR analysis identified the chemical structure of the synthesized materials within the 4000 –600 cm^{-1} range. Figure 1b displays broad O-H absorption bands at 3550 and 2900 cm^{-1}, indicating the stretching and bending vibrations of hydroxyl groups associated with water adsorption in the La_2O_3 lattice[23]. Sharp peaks at 1474 and 1362 cm^{-1} signify asymmetric and symmetric stretching of COO^- groups[24]. A band at 1055 cm^{-1} is associated with C–O stretching, while the band at 856 cm^{-1} corresponds to C–O bending. Lastly, the band at 650 cm^{-1} indicates La–O stretching vibrations, confirming the presence of La_2O_3 phases in the nanoparticle samples[25].

Brunauer–emmett–teller (BET) analysis

BET demonstrated a specific surface area of 18.89 m^2/g, indicating that the particles are very fine and resemble nanoparticles without internal porosity. The TEM/SEM results further confirmed the absence of porosity in the nanoparticles (Fig. 2).

Surface morphology and particle size measurement

Transmission electron microscopy (TEM)

Figure 2 shows TEM images revealing non-uniform, sheet-like structures and distinct aggregation patterns at 1 µm and 100 nm magnifications. TEM analysis revealed that the nanoparticles are primarily rod-shaped and spherical, with a hydrodynamic size of 128.871 ± 45.60 nm (SD) and a zeta potential of approximately 10.0675 ± 0.02586 mV when suspended in Milli-Q water. Sizes larger than 100 nm are likely due to aggregation resulting from their unique chemical and physical properties[26].

Body weight and general health analysis

Throughout the experimental period, the physical health and appearance of the mice were continuously monitored, and body weights were recorded. No significant changes in body weight were observed across the treatment groups during the two weeks and 35 days, as shown in Supplementary Figs. 1a and b. Similarly, the kidney indexes show no significant changes (Supplementary Figs. 1c and 1d). The equation was used to calculate the kidney indexes as referenced[27].

$$Kidney\ Index\ =\ (weight\ of\ left\ kidney\ (mg)/body\ weight\ (g))\ \times\ 100$$

Biomarkers for kidney injury and inflammation

SOD transcription elevated in chronic inflammation

To assess antioxidant activation in kidney tissues, the expression of the superoxide dismutase (SOD) gene was analyzed. After 14 days, SOD expression was significantly downregulated in kidneys treated with 150 mg/kg ($p \leq 0.0314$) and high doses (300 mg/kg, $p \leq 0.0061$) of lanthanum oxide nanoparticles (Fig. 3a). Conversely, after 35 days, SOD expression was significantly upregulated in kidneys treated with low (60 mg/kg) and medium (150 mg/kg) doses, with 66 and 104-fold increases, respectively, compared to the untreated control (Fig. 3b). Interestingly, SOD expression in the high-dose group (300 mg/kg) remained unchanged for 35 days. These findings suggest that the modulation of antioxidant responses is dose- and time-dependent.

GSH as an indicator of chronic kidney inflammation

After 35 days of exposure to nanoparticles, serum samples from mice showed a significant decrease in glutathione (GSH) levels, an essential antioxidant. Additionally, a strong negative correlation ($R^2 = 0.976$, $p < 0.0001$) was found between GSH levels and the concentration of nanoparticles (Fig. 3c). The control group exhibited GSH levels of 523.4 µg/g, compared to significantly lower levels in treated groups: 149.6 µg/g (60 mg/kg), 380 µg/g (150 mg/kg), and 463 µg/g (300 mg/kg). These results highlight chronic oxidative stress induced by prolonged exposure, particularly at lower nanoparticle concentrations.

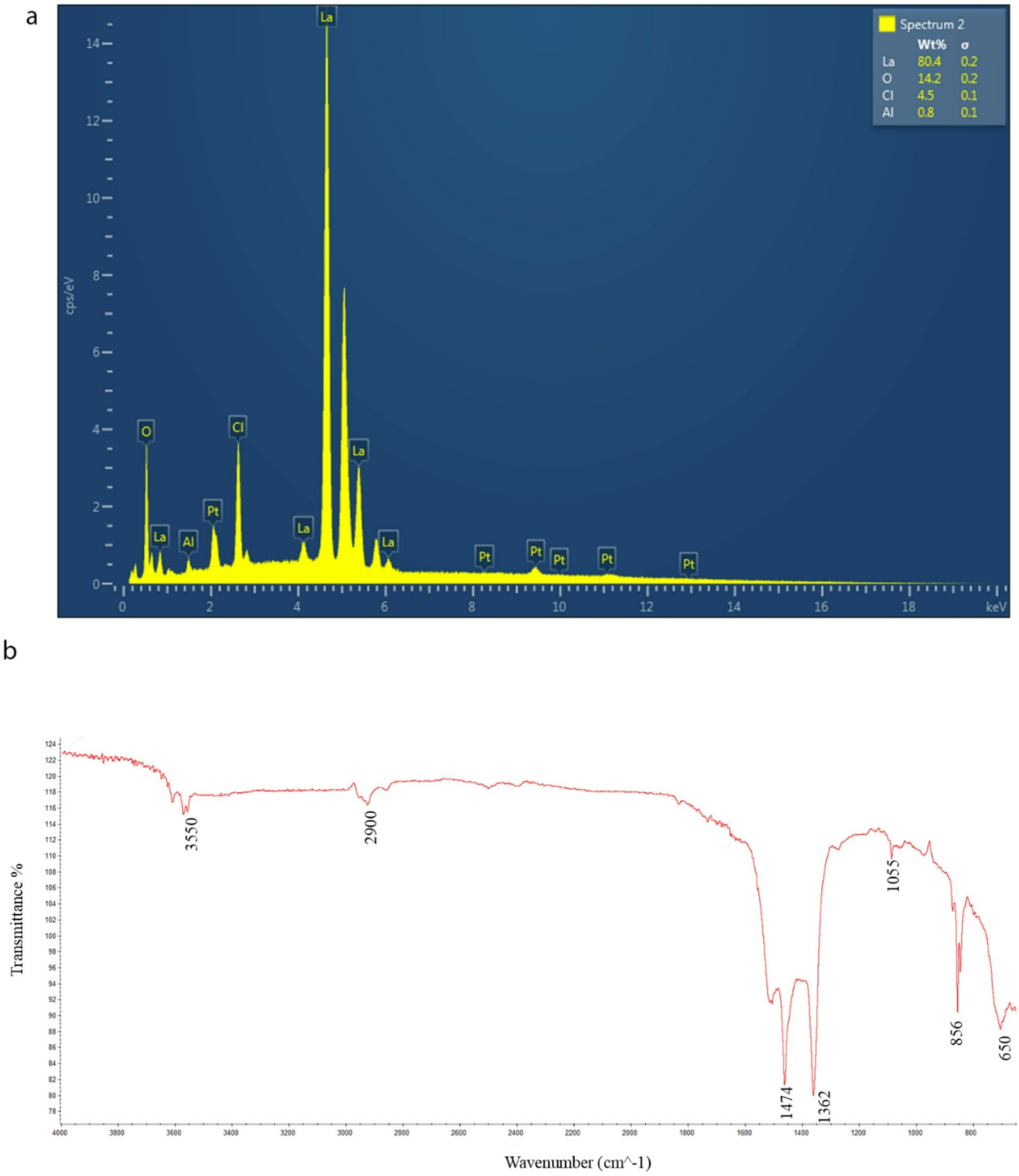

Fig. 1. **a**) EDS spectra of La_2O_3 NPs samples indicate the presence (wt%) of elements such as lanthanum, oxygen, aluminum, chlorine, and platinum. **b**) FTIR spectra of La_2O_3 NPs: List of infrared spectroscopy absorptions by frequency regions.

Acute inflammation marker NOS2 mRNA correlates with la_2o_3 NPs concentrations

The inducible nitric oxide synthase (iNOS, *NOS2*) gene, a biomarker for acute renal inflammation, exhibited significant amplification in the high-dose group (300 mg/kg) after 14 days, with a 4.89-fold increase ($p < 0.001$) compared to the control (Fig. 3d). After 35 days, NOS2 transcription levels were further elevated, reaching a 49.4-fold increase ($p = 0.0072$) in the high-dose group. Significant elevations were also observed in the low (10.9-fold) and medium (8.6-fold) dose groups at same time point (Fig. 3e). Linear regression analysis showed a strong

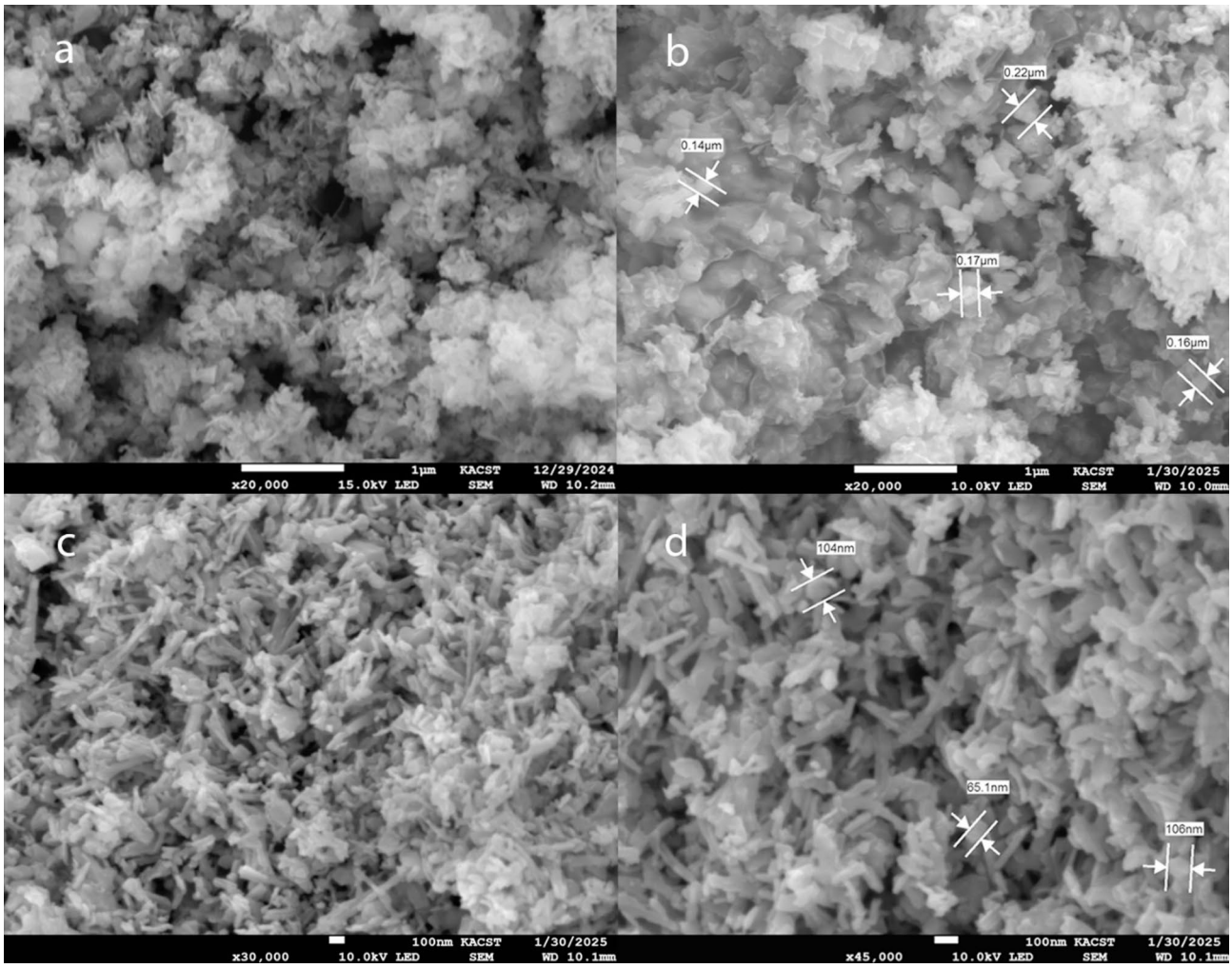

Fig. 2. SEM micrographs of the dispersed La_2O_3 NPs sample at magnifications (**a**) x20k, (**b**) x20k, (**c**) x30k, and (**d**) x45k. The nanoparticles mainly exhibit rod and spherical shapes, with a hydrodynamic size of 128.871 ± 45.60 nm (SD).

positive correlation between *NOS2* expression and nanoparticle concentration ($R^2 = 0.93$ at 14 days and $R^2 = 0.85$ at 35 days; Fig. 3f), supporting the nanoparticles' pro-inflammatory potential.

Upregulation of kidney injury molecule-1 (KIM-1) in a dose- and time-dependent manner

Kidney Injury Molecule-1 (*KIM-1*) gene expression, a sensitive marker for kidney damage, was significantly elevated in kidneys treated with the high dose (300 mg/kg) after 14 days ($p = 0.0007$; Fig. 3g). By day 35, KIM-1 transcription levels significantly increased across all doses, with fold changes of 24.3, 28, and 24.5 for the low, medium, and high doses, respectively ($p < 0.05$ for all groups; Fig. 3h). This consistent upregulation highlights the progressive kidney injury induced by lanthanum oxide nanoparticles.

Biochemical markers indicate tissue damage and inflammation

Kidney enzymes

Levels of uric acid and urea, key indicators of kidney function, were evaluated (Fig. 5). After 14 days, uric acid levels were elevated only in the medium-dose group (150 mg/kg), with a 4.7-fold increase ($p \leq 0.05$). By 35 days, significant increases in uric acid were observed in both the low-dose (60 mg/kg) and high-dose (300 mg/kg) groups, with 4-fold and 3.7-fold increases, respectively ($p = 0.0047$ and $p = 0.02$; Fig. 4a and b). Urea levels showed no significant changes in 14 days but were significantly elevated in all treatment groups after 35 days, with 60 mg/kg being the highest ($p < 0.05$; Fig. 4c and d).

Liver enzymes as indicators of systemic inflammation

The analysis of liver enzymes indicated systemic inflammation and the presence of nanoparticles. AST levels showed a significant rise only after 35 days with the lowest dose of nanoparticles (Figs. 5a and b); similarly, ALT levels were markedly elevated at both low and medium doses on day 35, with no changes observed at 300 mg/kg (Fig. 5c and d). The ALP test uniquely demonstrated substantial increases on day 14 at both 60 mg/kg and

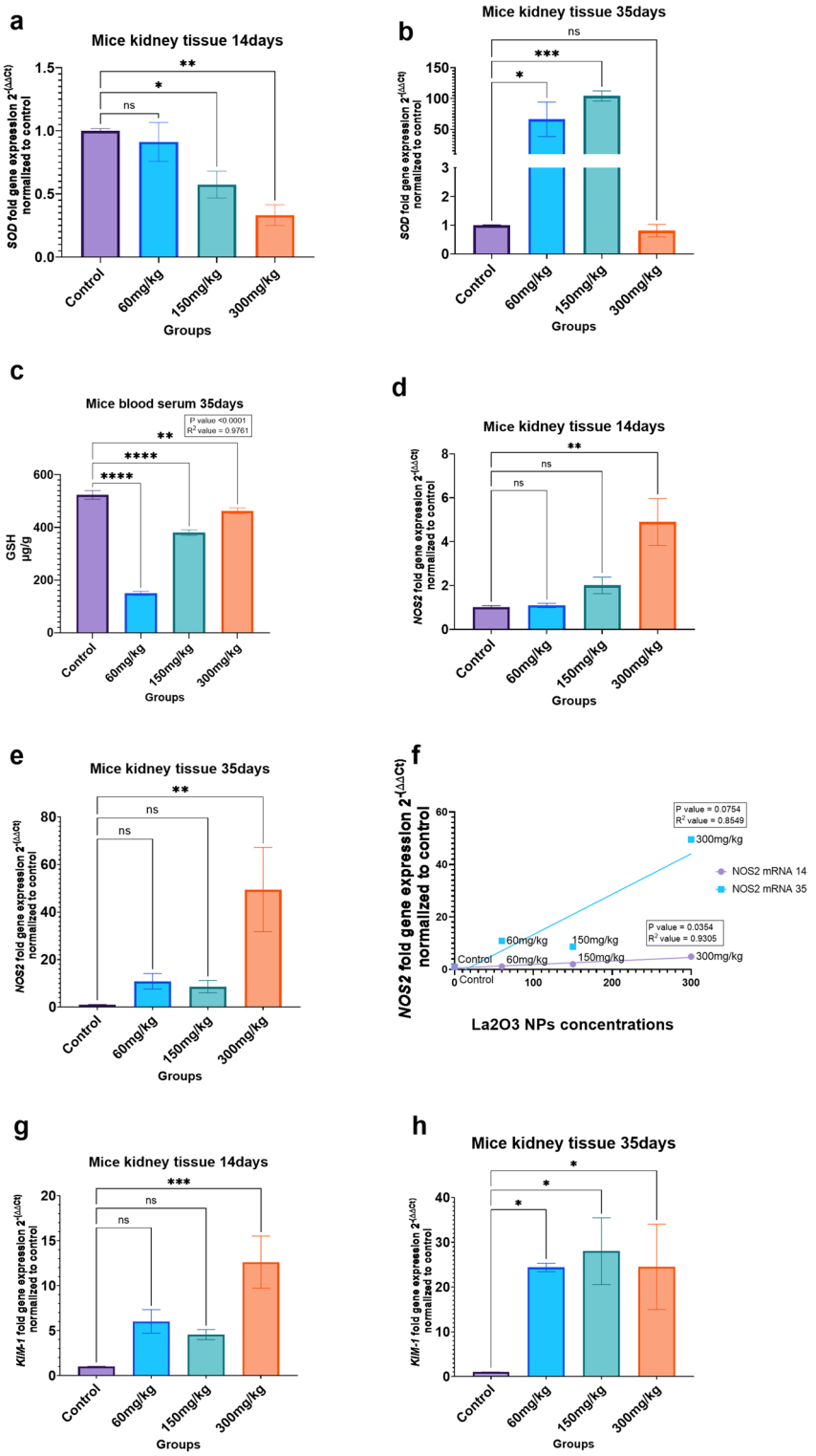

Fig. 3. Dose- and time-dependent effects of lanthanum oxide nanoparticles on gene expression in kidneys. **a**, and **b**) Fold changes in SOD gene expression relative to untreated controls after 14 and 35 days. A significant downregulation was observed at medium and high doses on day 14, while low and medium doses showed significant upregulation on day 35. **c**) GSH enzyme levels significantly decreased across all doses after 35 days, correlating negatively with nanoparticle concentration. **d**, and **e**) NOS2 gene expression amplified in the high-dose group after 14 and 35 days, with significant elevations at lower doses on day 35. **f**) Pearson regression analysis showed a positive correlation between NOS2 transcription and nanoparticle concentrations at both time points. **g** and **h**) KIM-1 gene expression significantly increased at high doses on day 14 and across all doses on day 35. Data representing the mean ± SEM. *$p < 0.05$, ** $p < 0.01$, ***$p < 0.001$, and ****$p < 0.0001$ were considered significant using one-way ANOVA and the Dunnett post-hoc test; ns (not significant). RT-qPCR was performed in duplicate with biological triplicate.

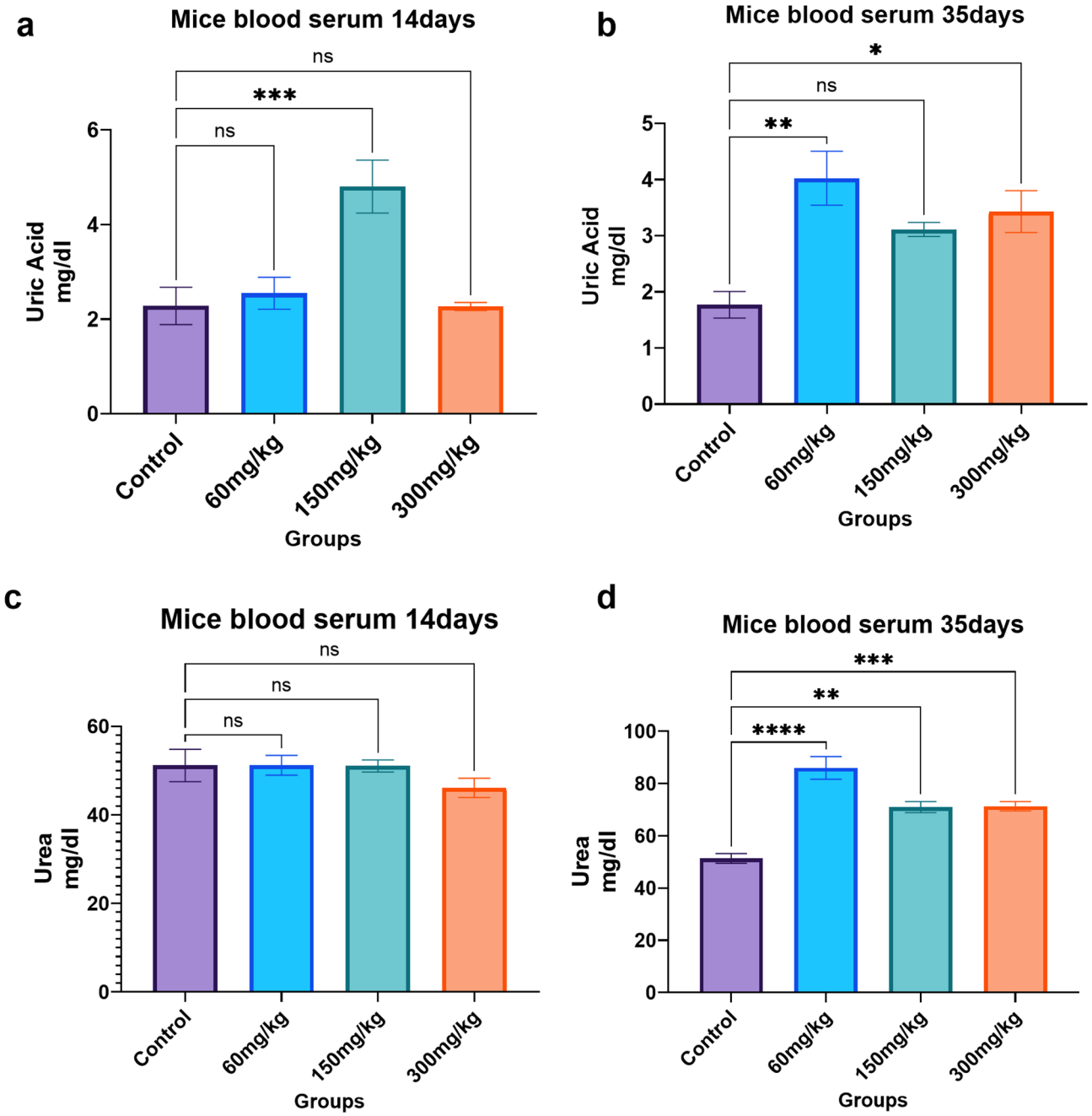

Fig. 4. Kidney enzyme activity reflects tissue damage and inflammation. **a** and **b**) Uric acid levels were significantly elevated at medium doses on day 14 and low and high doses on day 35. **c**, and **d**) Urea accumulation showed no significant changes on day 14 but increased significantly across all doses by day 35. Data representing the mean ± SEM. *$p < 0.05$, ** $p < 0.01$, ***$p < 0.001$, and ****$p < 0.0001$ (in triplicate) were considered statistically significant using one-way ANOVA and the Dunnett post-hoc test; ns (not significant).

300 mg/kg doses, but by day 35, only the 60 mg/kg dose maintained this elevation and even increased (Fig. 5e and f). Finally, a negative correlation was found between GSH levels and liver enzyme activity, suggesting that oxidative stress resulting from nanoparticle exposure is linked to liver damage, with the most significant effects observed at 60 mg/kg and the least impact at 300 mg/kg, illustrated in Fig. 5g.

Sustained inflammation and cytokine signaling pathway activation

Chronic inflammation markers in low-dose groups (60 mg/kg)

Kidney lysates from mice exposed to low doses of lanthanum oxide nanoparticles (60 mg/kg) showed a sustained increase in inflammatory cytokines over both time points (14 and 35 days). Using the Mouse Cytokine Antibody Array, the highest protein expressions were observed for BH3 interacting domain death agonist (BID), BCL2-associated X protein (BAX), and insulin-like growth factor 2 (IGF-2) in the 14-day samples (Fig. 6a). These

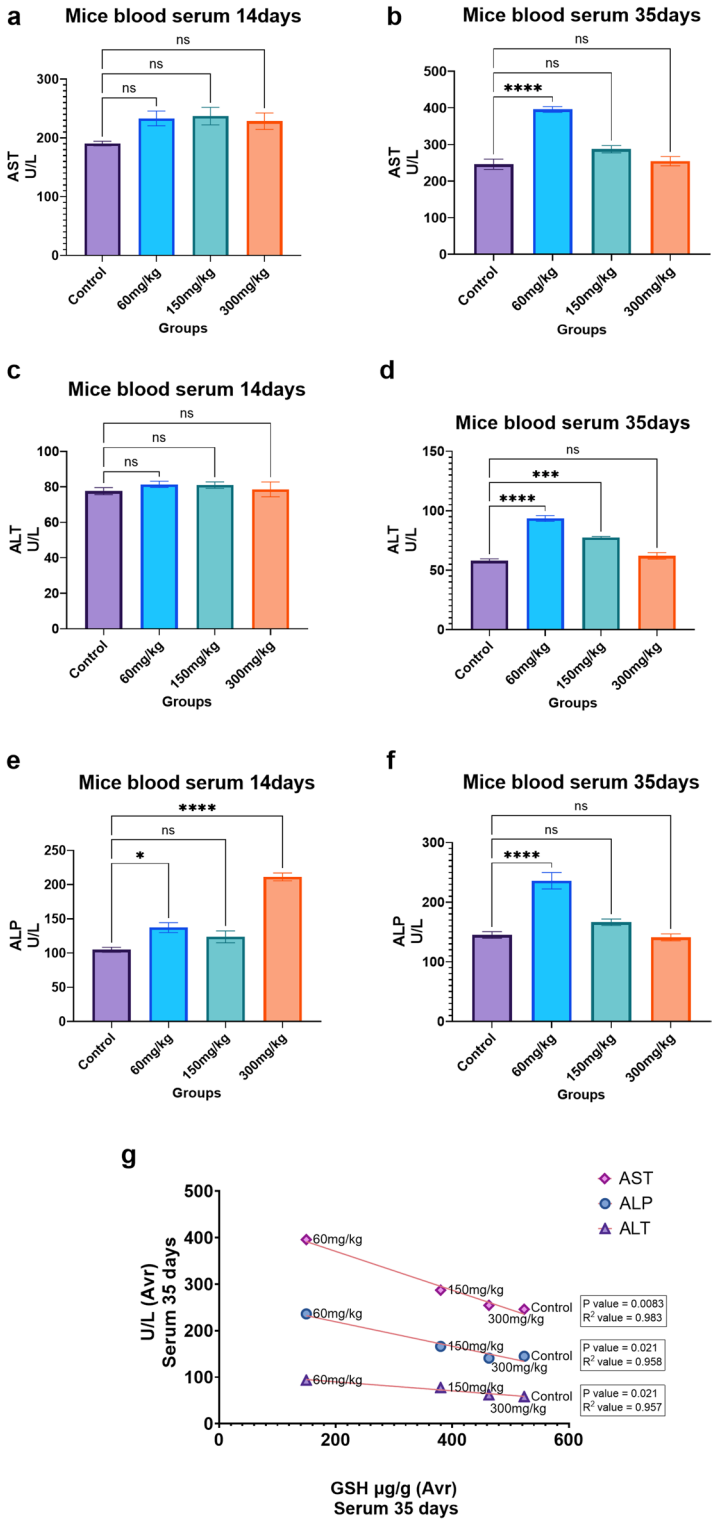

Fig. 5. Liver enzyme levels indicate systemic inflammation. **a**, and **b**) AST levels increased significantly at low and medium doses after 35 days. **c**, and **d**) ALT levels showed significant elevations at low and medium doses on day 35, with no changes on day 14. **e**, and **f**) ALP levels increased at low and high doses on day 14, with sustained elevations at low doses on day 35. **g**) Pearson regression analysis revealed a strong negative correlation between GSH levels and liver enzyme activity. Data representing the mean ± SEM. $^{*}p < 0.05$, $^{**}p < 0.001$, and $^{***}p < 0.0001$ (in triplicate) were considered statistically significant using one-way ANOVA and the Dunnett post-hoc test, ns (not significant).

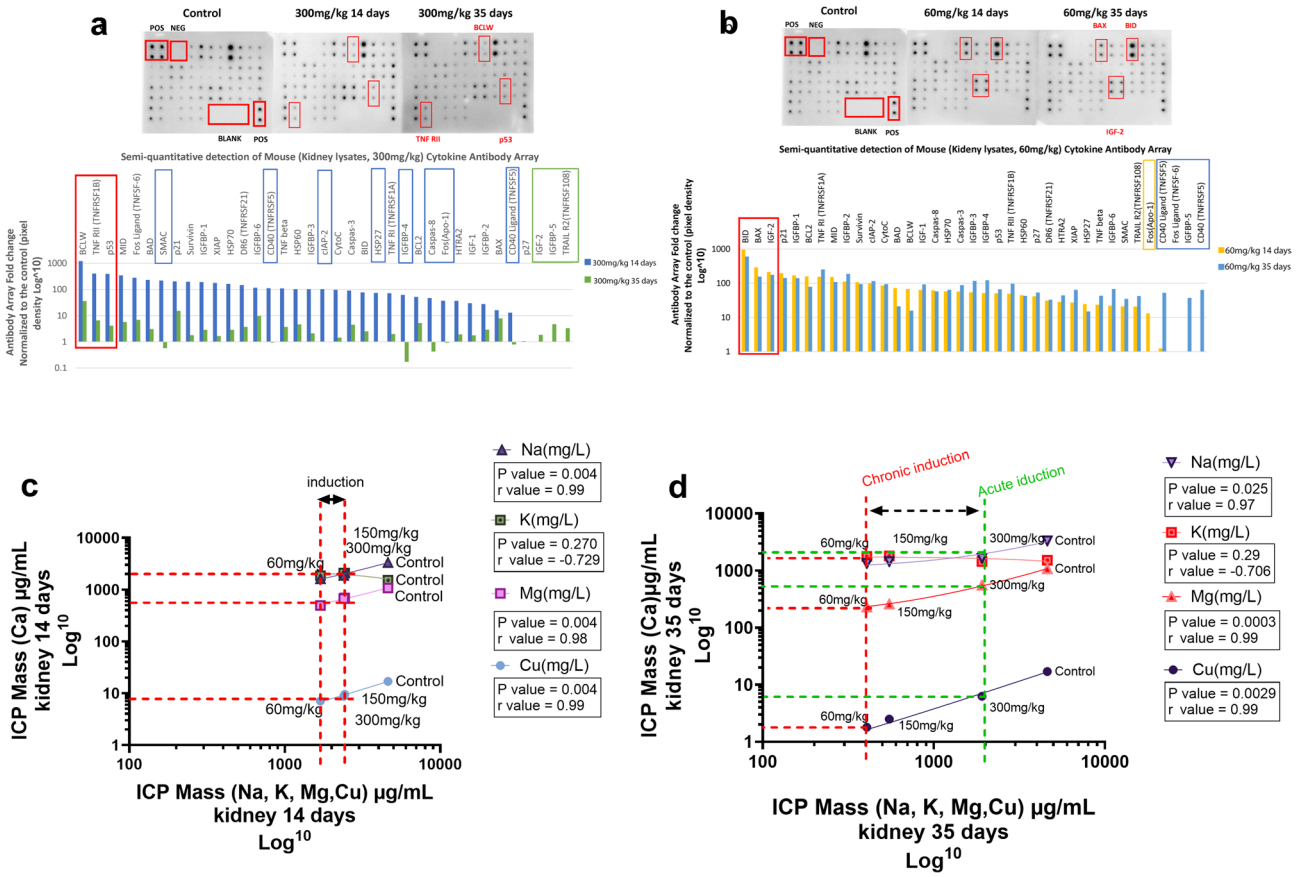

Fig. 6. La_2O_3 nanoparticles activate the kidney's cytokines response and describe Ca homeostasis. **a**) Mouse cytokine array images show fold changes relative to control, comparing treatment with 60 mg/kg nanoparticles for 14 and 35 days. BID, BAX, and IGF-2 proteins increased in 14-day samples, while CD40 ligand, IGF2BP-5, and CD40 were prominent at 35 days. FOS (Apo-1) expression peaked at 14 days but fell by 35 days. **b**) Cytokine array images of kidney lysates treated with 300 mg/kg nanoparticles for 14 and 35 days. Protein levels rose in 14 days, including BCL-W, TNFRII, and p53, then decreased by 35 days. Data show fold changes in inflammatory cytokine levels, with transient SMAC, cIAP-2, and HSP27 elevations on day 14. Sustained expression of IGF-2, IGF2BP-5, and TRAIL-R2 were noted at 35 days. **c**) Pearson analysis showed a significant and positive correlation between Ca, Na, Mg, and Cu mineral concentrations after 14 days, arranged as follows: 60 mg/L (the lowest), control (the highest), and 150 and 300 mg/kg in between. However, a negative correlation of -0.72 was observed with K. d) Pearson correlation and simple linear regression revealed a negative correlation between Ca and K ions ($p = 0.29$, $r = -0.706$) after 35 days of exposure. Over time, the Na, Mg, and Cu mineral concentrations continued to decrease, surpassing 300 mg/kg, resulting in a severe progression of induction, where 300 mg/kg exhibited an acute effect. One-way ANOVA, the Dennett post-hoc test, Pearson Correlation, and simple linear regression ($n = 3$) were used.

proteins remained elevated at 35 days, with increased CD40 ligand, IGF2-binding protein 5, and CD40 (Fig. 6a). The expression of FOS (Apo-1), a proto-oncogene transcription factor, peaked at 14 days but declined at 35 days, consistent with its role in acute inflammatory responses.

Interestingly, the loss of FOS ligand (TNFSF-6) across both time points indicates a potential limitation in the adaptive response to nanoparticle-induced inflammation. These findings suggest that low doses of nanoparticles promote chronic inflammation by sustaining cytokine signaling and apoptotic pathways.

Acute and resolving inflammatory responses in high-dose groups (300 mg/kg)

In contrast to the sustained inflammation observed at low doses, cytokine profiles in high-dose groups (300 mg/kg) revealed acute but transient inflammatory responses. After 14 days, the most highly expressed proteins included BCL-W, tumor necrosis factor receptor II (TNFRII), and p53, all associated with apoptosis and immune activation (Fig. 6b). However, by 35 days, the expression of these proteins significantly decreased, indicating a resolution of acute inflammation.

Notably, proteins such as second mitochondria-derived activator of caspases (SMAC), cellular inhibitor of apoptosis protein 2 (cIAP-2), and heat shock protein 27 (HSP27), which were elevated at 14 days, returned to baseline by 35 days (Fig. 6b). This decline suggests that higher nanoparticle concentrations may trigger an adaptive response to mitigate prolonged inflammation.

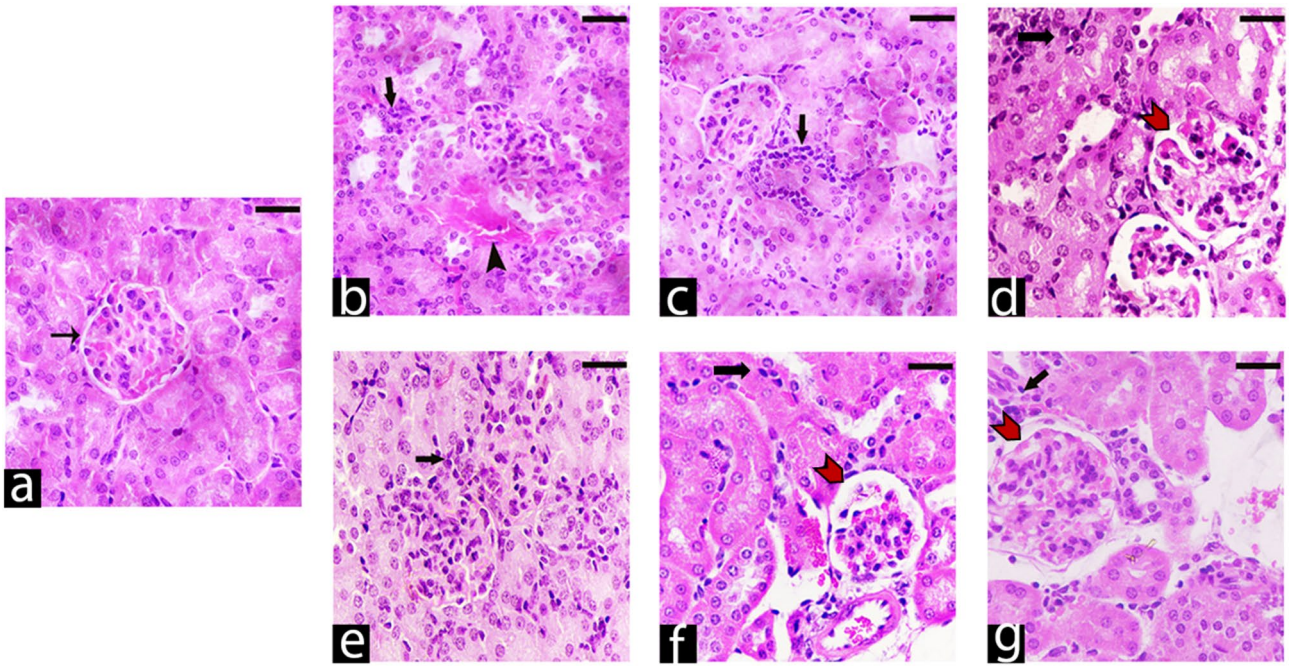

Fig. 7. Photomicrographs of hematoxylin and eosin (H&E)-stained kidney sections after 14 and 35 days. (**a**) Represents the control group illustrating normal glomerulus (thin arrow). (**b**) Displays La_2O_3 NPs 60 mg/kg for 14 days, showing inflammatory cells around the glomerulus (thick arrow). (**c**) La_2O_3 NPs (150 mg/kg) administered for 14 days resulted in exposed mice exhibiting noticeable features, including hemorrhage (black arrowhead) and inflammatory cells (arrow). (**d**) La_2O_3 NPs (300 mg/kg) for 14 days, illustrating inflammatory cells (arrow) and Glomerular atrophy (red arrowhead). (**e**) Displays La_2O_3 60 mg/kg for 35 days, showing inflammatory cells (arrow). (**f**) Mice exposed to La_2O_3 NPs (150 mg/kg) for 35 days showed noticeable features, including inflammatory cells (thick arrow). Glomerular atrophy (indicated by the red arrowhead) was also observed. (**g**) La_2O_3 NPs (300 mg/kg) administered for 35 days resulted in glomerular atrophy and degeneration of some renal tubules. Scale bar = 200 µm.

Mineral distribution and ion homeostasis

Calcium and potassium imbalances

Lanthanum oxide nanoparticles significantly disrupt mineral homeostasis, particularly calcium and potassium levels (Fig. 6c and d). After 14 days, calcium levels in (0.5 g) kidney tissues dropped nearly 3000-fold in the low-dose group (60 mg/kg, $p < 0.011$) and 2000-fold in medium- and high-dose groups (150 and 300 mg/kg, $p < 0.04$; Supplementary Fig. 3A). Correspondingly, potassium levels increased significantly, with mean differences of 1854 µg/mL (low dose), 2100 µg/mL (medium dose), and 2097 µg/mL (high dose) compared to the control (Supplementary Fig. 2).

After 35 days, calcium loss was amplified, with reductions of up to 4000-fold at low and medium doses. Potassium levels normalized over time in all groups except the high-dose group, where elevated potassium persisted (Supplementary Figs. 3). This suggests a slower or incomplete recovery of ion homeostasis at lower NPs concentrations.

Sodium and magnesium imbalances

Sodium levels significantly decreased in the high- and low-dose groups, showing a 2- to 3-fold reduction compared to controls after 14 and 35 days ($p < 0.05$; Supplementary Fig. 4A). Magnesium and copper levels followed a similar pattern, showing consistent reductions in conjunction with calcium at all time points, indicating a widespread disruption of essential minerals.

Linear regression analysis revealed a strong positive correlation between calcium and other minerals, including sodium, magnesium, and copper ($R^2 = 0.99$, $p < 0.004$), as well as a negative correlation with potassium ($R^2 = -0.72$, $p = 0.029$). These results suggest that lanthanum oxide nanoparticles mimic calcium ions, disrupting ion channels and mineral homeostasis in a dose- and time-dependent manner (Fig. 6c and d).

Histopathological assessments of kidney damage

The histopathology examination (40x) of the kidneys treated with La_2O_3 NPs showed significant degradation compared to the control at all doses and time points (Fig. 7). The renal cortex in the control group exhibited a typical tissue architecture characterized by intact tubules and glomeruli (Fig. 7a). However, in Fig. 7b and d, sections treated with NPs showed general atrophy of the renal capsule, wide spacing of tubules, severe infiltration of inflammatory cells, and hemorrhage, which worsened over time. A similar but more pronounced impact of

NPs damage, characterized by tubular dilatation, desquamation, vacuolation, necrosis, and debris buildup in the tubular lumina with inflammatory cell infiltration, was still observed after 35 days (Figs. 7e—7 g).

Discussion

This study aimed to investigate the nephrotoxic effects of lanthanum oxide nanoparticles using a dose- and time-dependent approach. Our findings reveal significant kidney dysfunction and inflammation associated with La_2O_3 NP exposure, emphasizing their potential to disrupt mineral homeostasis, induce oxidative stress, and activate inflammatory signaling pathways. These results align with and expand on previous research, offering new insights into the mechanisms underlying La_2O_3 NP-induced toxicity during filtration. This is particularly important due to the increased release of these nanoparticles in the environment as a result of their growing use in various products, such as electronics manufacturing and as antimicrobial agents[4,5,28,29].

We characterized the nanoparticles' size, surface properties, and chemical composition, confirming that they are primarily non-porous and rod-shaped, with hydrophilic surfaces containing -OH and -COOH functional groups. Previous studies indicate that these rod-shaped nanoparticles enhance cellular interactions due to their higher surface-to-volume ratio and improved alignment with cell membranes. Their hydrophilic surfaces also facilitate cell adhesion by promoting protein adsorption and providing binding sites for cell receptors[30–32].

In this study, we administered single intraperitoneal injections of La_2O_3 nanoparticles to female Swiss albino mice at doses of 60, 150, and 300 mg/kg body weight, observing the effects at 14 and 35 days. Studies have shown the i.p. induction ensures accurate nanoparticle concentration and dosage, as oral or gavage methods can lead to inaccurate results, particularly with poorly absorbed drugs identified at very low concentrations in body fluids and tissues, which could be misleading[33,34]. Our research showed that a single i.p. dose of nanoparticles caused liver damage in mice after one week, consistent with other studies using oral or inhalation methods. Although no significant physical changes or body weight differences were observed compared to the control group, there was a notable effect on body metabolism. These results align with studies administering oral doses of 1 to 100 mg/kg for 30 or 60 days[35,36], suggesting that La_2O_3 NPs do not hinder growth and development in female mice, unlike lanthanum chloride ($LaCl_3$) NPs[37].

It's essential to confirm the impact of Lanthanum oxide nanoparticles through histopathologic assessment and the analysis of kidney biomarkers. Previous studies have demonstrated that imbalances in oxidants and antioxidant enzymes correlate with atrophy of the renal capsule, wide spacing of tubules, severe infiltration of inflammatory cells, and hemorrhage. These factors can trigger cell death and inflammation, making them valuable as injury biomarkers, especially in kidney health[38–40].

We compared gene expression results at different concentrations over time, specifically after two weeks and again after 35 days. SOD expression was significantly reduced in 14 days in mice treated with medium and high doses (150 and 300 mg/kg) but increased at lower doses (60 mg/kg) after 35 days. This fluctuation reflects a dual-phase response where early oxidative stress suppresses antioxidant activity while prolonged exposure induces compensatory mechanisms. Moreover, conflicting reports in the literature regarding SOD as a reliable CKD marker highlight the need to consider other markers, such as GSH, in conjunction[41–45]. GSH, a major non-enzymatic antioxidant, decreases with CKD, making it a more reliable marker of antioxidant status. Interestingly, our data indicate a significant loss of GSH in the plasma, which strongly correlates with the concentration of NPs. The loss of GSH was highest at 60 mg/kg NPs and lowest at 300 mg/kg, with only an 11.5% loss. This also agreed with Li et al., that the NPs generate ROS and nitrogen species (RNS) that harm the tissue severely by interacting with the macromolecules and disrupting the cell hemostasis[46]. Prolonged exposure to 60 mg/kg of La_2O_3 NPs worsens kidney inflammation, as indicated by decreased plasma levels of glutathione GSH and increased transcription levels of SOD in kidney tissue after 35 days. In contrast, exposure to 300 mg/kg showed a lower impact, likely due to nanoparticle aggregation that reduces their interaction with cellular macromolecules, which aligns with Shang et al.'s findings that higher concentrations lead to decreased nanoparticle uptake[47]. Also, our previous work, Almukhlafi et al. (2021), noted that this property may disrupt cellular ion homeostasis. The nanoparticles' stoichiometric integrity, confirmed through TEM and ROS analysis, ensures they retain their physicochemical properties, influencing their ability to penetrate cell membranes and interact with intracellular components[48].

In addition, we analyze the serum for liver enzymes, which are intensively studied in the literature, that lanthanum oxide nanoparticles cause hepatotoxicity[12]. A strong connection between nanoparticles and histopathological changes has been noted in the literature, highlighting severe inflammation in the livers of mice[36,48–50]. The liver is the primary source of GSH, playing a central role in maintaining GSH homeostasis by exporting nearly all synthesized GSH into plasma and bile[51]. Liver enzymes such as ALP, ALT, and AST are reliable markers for assessing liver function. An increase in these enzymes indicates liver stress and potential hepatic dysfunction[52]. There is a significant increase in AST and ALT levels in the NP-treated groups after prolonged exposure. ALP enzyme levels rose in both low and high-dosage groups after 14 days. After 35 days, ALP levels increased further, indicating that the lower concentration had more significant damage. Remarkably, we observed a negative correlation between GSH levels and liver enzymes, suggesting that as GSH levels decreased, these liver enzymes increased, and vice versa. This is consistent with the effects of Cadmium-induced hepatotoxicity in rats. Cadmium is a hazardous toxin that promotes liver damage by increasing liver enzymes and reducing GSH levels in rats[53]. Our work demonstrated the impact of La_2O_3 NPs on the livers of mice, specifically in terms of ROS, in response to varying NP concentrations, with the most damage observed at the lowest dose of 60 mg/kg and the least hepatotoxicity at 300 mg/kg.

The accumulation of ROS over time can increase pro-inflammatory cytokines and inducible NOS2 expression, worsening inflammation and creating a vicious cycle[54,55]. Udi and his team found that activating the iNOS signaling pathway via cannabinoid receptors in the kidney can lead to renal dysfunction and fibrosis, particularly in patients with kidney disorders[56]. This investigation, related to these studies, demonstrated a

significant increase in *NOS2*, showing a strong correlation between NOS2 transcription and NP concentration. This effect is observed significantly with the highest dosage (300 mg/kg) before the low and mid-NP dosages on day 14, demonstrating that 300 mg/kg is the first to induce Acute Kidney Injury (AKI). Moreover, a study published in 2024 highlighted the significant impact of iNOS as a biomarker for the activation of inflammation in kidney tissue, causing the first stage of CKD, which can be reversed if treated, known as AKI[57].

Another biomarker for AKI we used was KIM-1, which exhibits significant upregulation in proximal renal tubular cells in response to ischemic or nephrotoxic acute kidney injury[58]. In our investigation of La_2O_3 NPs, we observed that after 14 days of exposure at 300 mg/kg, mice exhibited a significant increase in *KIM-1* levels in their kidneys, suggesting the activation through physical aggregation. By 35 days, all concentration tests demonstrated a substantial increase in kidney injury, as indicated by monitoring *KIM-1* and *NOS2* transcription. Comparable results were observed when evaluating the impact of AgNP and CuO NPs' toxicity in rat kidneys, causing severe nephrotoxicity via KIM-1, Uric Acid, and Urea elevation, along with a sharp decrease in SOD and GSH enzymes[59,60].

A crucial marker of kidney failure is uric acid accumulation in the blood, and research has suggested that it activates inflammatory pathways and initiates AKI[61]. We assessed the uric acid levels and observed a substantial increase in mice treated with 150 mg/kg for 14 days. Nevertheless, in 35 days, the 60 and 300 mg/kg dosages treated in groups significantly increased blood uric acid levels. Furthermore, urea accumulation increased at all concentrations after 35 days, with no notable change at any NP concentrations on day 14. Usually, the accumulation of urea is prevalent in cases of moderate-to-advanced CKD[62]. Fadia et al. conducted a histopathological investigation on the kidneys of rats exposed to Gold nanoparticles (GNPs), revealing kidney injury, increased urea in all rats, and uric acid at 100 and 250 mg/kg GNPs[52]. As mentioned above, metal nanoparticles can lead to harmful changes in kidney tissues (nephrons), causing elevated uric acid and urea levels in the bloodstreams of mice and rats. However, the severity of these effects varies based on the size, dose, and duration of exposure.

Moreover, we assess the impact of La_2O_3 nanoparticles on cytokine responses, which can cause inflammation and cell death when administered intraperitoneally. To illustrate the unique characteristics of the nanoparticles and the protein activation cascade, we used Mouse Cytokine Antibody Arrays to examine the effects on the exposed kidney lysates. We target the lowest and highest concentrations (60 mg/kg and 300 mg/kg) for 14 and 35 days, excluding the 150 mg/kg dose, as it yields intermediate results between the selected dosages.

Based on the time duration and concentration, we compared the results of protein expression from the array with the starting point, two weeks, and the endpoint after 35 days. The protein expression levels were highest for BID, BAX, and IGF-2, particularly in the start-point kidney lysate treated with 60 mg/kg, indicating apoptosis[63,64]. Similarly, IGF2 plays a significant role in cell survival and apoptosis through the Akt pathway, and knocking down *IGF2* impairs mitochondrial functions and causes mitochondrial ROS accumulation[64,65]. The dysregulated IGF system is associated with kidney diseases such as CKD and plays a role in kidney growth, structure, and function. It consists of IGF-1 and IGF-2, and the overabundance may encourage the development of tumor cells and hinder the elimination of damaged cells[66]. Our exploration confirms the activation of intrinsic apoptosis, as other final protein products were also expressed, including BCL2, TNF, CytoC, BAD, IGF-1, Caspase-8/3, and p53; this could be attributed to the exposure to NP. In a previous study, Sisler et al. demonstrated that inhalation of cobalt monoxide (CoO) and lanthanum oxide nanoparticles at a concentration of 30 mg/m^3 elicited a distinct inflammatory response in the lungs. After 56 days of exposure, only La_2O_3 induced a chronic inflammatory and fibrogenic response, with more persistent inflammation compared to CoO, which caused acute inflammatory symptoms[67]. Our data showed that mice treated with 60 mg/kg of La_2O_3 NPs exhibited a sustained elevation from the start to the endpoint, activating the cytokine signaling pathway and displaying a chronic inflammation response similar to that investigated by Sisler et al.

Related to the nephrons, both arrays treated with 60 mg/kg La_2O_3 NPs indicate simultaneous changes between two-time points, but only the FOS (Apo-1) protein experiences an increase at the start point and then a protein loss at the endpoint. The upregulation of this transcription factor is related to nephrotoxic murine AKI and induced by folic acid or cisplatin in proximal tubular cells exposed to TNFα, a cytokine that mediates AKI[68]. This research demonstrated that the rise in FOS (Apo-1) is a component of the kidney's protective response to injury, which helps maintain Klotho, reduces the inflammatory response, and limits damage to tubular cells and the kidney in vivo. Moreover, the same group has shown equivalent results in vitro using mouse kidney cells and confirmed time restraint for the transcription expression. It significantly elevated after 4 h and gradually started to decline after 12 h, reaching basal levels after two days, indicating the primary function in limiting further response[69]. Indeed, we found that exposure to 60 mg/kg La_2O_3 NPs can act as inflammatory mediators elevating many TNF family members in the kidney that initiate AKI characterization and activate FOS (Apo-1), but only at the start point (14 days), as an adaptive response to limit the inflammation with the loss of IGF2BP-5 and vice versa after 35 days. IGF2BP-5 is a family member that promotes IGF signaling, as mentioned above. In addition, similar results were observed in array samples treated with 300 mg/kg, showing elevated levels at the beginning and a loss at the end for FOS (Apo-1), compared to the untreated samples, and vice versa, with lower IGF2BP-5 expression.

Next, the 300 mg/kg La_2O_3-treated group exhibited distinct protein array results at two time points, indicating reduced inflammation and cytokine levels after 35 days. The increase in expression at shorter exposure times is evident in BCLW, TNFRII, and p53 proteins. According to our published study, lanthanum oxide nanoparticles significantly impact pro-apoptotic and anti-apoptotic proteins, leading to an imbalance in the p53/BCL-2 protein ratio and changes in Caspase 3 gene expression[12]. This suggests that a struggle for cell survival depends on p53 to activate many signaling cascades that cause immediate cell death in the kidneys, including Caspase, SMAC, and cIAP-2[70–72]. p53 is critical in AKI and CKD by promoting renal tubular injury in response to cellular stress, ultimately leading to apoptosis[73]. Moreover, the scientific community believes that the TNF family significantly

contributes to renal damage despite its potential for kidney protection. Targeted therapeutics inhibiting specific TNF receptors (TNFRI or TNFRII) in animal models could help balance TNF's effects in renal disease, offering improved clinical profiles[74–76]. Our data indicate that BCLW, TNFRII, and p53 showed a rapid increase at the start point when treated with 300 mg/kg of elevated Caspase proteins; however, after 35 days, a sharp decrease in the mentioned proteins, accompanied by low Caspase, SMAC, and cIAP-2 expression, might indicate AKI characterization.

Another known adaptive response that protects the kidney tissue is Heat shock protein 27 (HSP27), especially against cellular changes associated with ischemia-reperfusion injury (IRI)[77–79]. This chaperone protein is an antioxidant and is crucial in regulating apoptosis. Due to its pro-survival activity, metal nanoparticles, such as gold nanoparticles, exhibit neuroprotective ability against Amyloid-beta (Aβ) peptide-induced inflammation by upregulating HSP27[80]. Furthermore, the oral gavage of 200 mg/kg Copper NPs for five days caused severe nephrotoxicity. Caused by the upregulation of the HSP27 gene in rats' kidneys, activating the Mitogen-activated protein kinase (MAPK) and insulin signaling pathways in response to stress and inflammation[81]. As determined by the array, we also identified La_2O_3 NPs as causing cellular stress, including oxidative stress and inflammation, particularly in the other HSP family. Nonetheless, only the highest concentration (300 mg/kg) showed a rapid loss in expression at the endpoint. Then again, a recent study has demonstrated that the inhibition of the HSP family is a positive indicator of cell death when cells are treated with synthesized Macrolepiota procera mushrooms bound with silver nanoparticles[82]. They believe it has a similar impact to 17-AAG and Debio-0932, a known HSP90 inhibitor that activates the intrinsic apoptotic pathway *via* the activation of p53/BAX expression[83,84]. Remarkably, our data show BAX sustains even after 35 days, and the loss of other HSP family members, such as HSP70 and HSP60, further confirms our results. We hypothesized that losing HSF family members due to 300 mg/kg exposure for 35 days shifted the apoptotic pathways from extrinsic to intrinsic activation of cell death. This may explain the general downregulation of the cytokine inflammatory protein array; however, further studies are still required to confirm this.

The mechanism by which La_2O_3 NPs induce the ROS and inflammation pathway has yet to be fully understood. The nanoparticles are believed to produce ROS, which triggers cell death pathways after they enter the cell membrane, releasing La^{3+} ions that act like calcium (Ca^{2+}) and disrupt several metabolic processes[35,36,48,85]. Studies have also indicated that the toxic effects of La_2O_3 NPs in *vivo* and in *vitro* may be due to free La^{3+} ions and their activation of the intrinsic mitochondrial pathway and autophagy, an alternative pathway to cell death that is not dependent on apoptosis [8,11,86]. Dressler et al. demonstrated a significant decrease in calcium levels by analyzing the femur bone of rats administered different doses of La_2O_3 orally, which showed a positive correlation with sulfur, zinc, nickel, sodium, and copper and the loss of calcium. However, the direct impact of this mineral disruption on intrinsic and extrinsic apoptosis has not been studied[36]. Like the findings of Dressler et al. (2020), our study highlights a significant reduction in calcium levels over time after the administration of La_2O_3, which is correlated with other minerals such as sodium, potassium, magnesium, and copper. Additionally, our study suggests that La_2O_3 nanoparticle exhibits characteristics that can lead to kidney damage by triggering inflammation and activating intrinsic and extrinsic apoptosis, utilizing inorganic elements as biomarkers. Unfortunately, unlike Cadmium, the literature is significantly lacking regarding the interaction between La_2O_3 and calcium in the body. This heavy metal has been extensively studied concerning calcium and its protective effects against Cadmium accumulation in the liver and kidneys[87,88]. Additionally, when a calcium deficiency occurs, Cadmium ions efficiently bind to calcium-binding protein (CaBP) and transport it into the bloodstream without competing with calcium[89]. As the La_2O_3 concentration decreased, the La^{3+} interaction decreased, thereby reducing the competition between the NP ions for binding to the CaBP cell, which caused more damage. This can be seen as calcium loss, ROS, and inflammation at the lowest NP concentration (60 mg/kg NPs), with the most damage progressing over time. La^{3+} inhibits myocytes' Na^+/Ca^{2+} exchange activity and other Ca^{2+} transport processes. The study showed that a small amount of La^{3+} can increase the exchange-mediated influx of Ca^{2+} by 20-fold, but cytosolic La^{3+} partially inhibits Ca^{2+} uptake[90]. This describes the loss of Ca^{2+} in kidney lysate over time, which correlated inversely with NP concentration.

Our data indicate that La^{3+} ions contribute significantly to the observed effects; however, we must consider the dissolution kinetics of La_2O_3 NPs under the experimental conditions. Previous studies have demonstrated that La_2O_3 NPs partially dissolve in acidic or ligand-rich environments, releasing La^{3+} ions[91,92]. In physiological media at pH ~ 7.4, these ions will likely precipitate as phosphates or carbonates, limiting their bioavailability[93,94]. Future research is essential to quantifying La_2O_3 NP dissolution and comparing biological responses to ionic La^{3+} controls, which will clarify the specific effects of these particles.

In summary, the response to La_2O_3 depends on the concentration and duration of nanoparticle exposure. This damage may be attributed to NP La^{3+} ions, which mimic calcium and amplify ROS production at lower concentrations. Finally, this results in ROS, cytokines, inflammation, and kidney histopathological damage, which intensifies at the lowest dose.

Conclusions

These findings suggest that the unique properties of the nanoparticles likely contribute to the harmful effects of La_2O_3 on the kidneys. These properties contribute to nephrotoxicity, which is influenced by exposure dose and duration. These properties trigger the production of ROS, and manipulation of Ca^{2+} homeostasis leads to cytokine activity and chronic kidney disease at various stages and levels of severity. However, further research is needed to determine whether these effects result from direct nanoparticle circulation or secondary toxicity mechanisms.

Data availability

The data supporting this study's findings are available from the corresponding author upon reasonable request.

Received: 20 February 2025; Accepted: 30 May 2025
Published online: 06 June 2025

References

1. Alyami, N. M., Almeer, R. & Alyami, H. M. Role of green synthesized platinum nanoparticles in cytotoxicity, oxidative stress, and apoptosis of human colon cancer cells (HCT-116). *Heliyon* **8** (12), e11917 (2022).
2. Almasoud, H. A. et al. *Dose-Dependent Variation in Anticancer Activity of Hexane and Chloroform Extracts of Field Horsetail Plant on Human Hepatocarcinoma Cells*2022p. 5778411 (BioMed Research International, 2022). 1.
3. Martins, A. et al. *Enhanced cytotoxicity against a pancreatic Cancer cell line combining radiation and gold nanoparticles. Pharmaceutics*, **16**(7). (2024).
4. Li, Y. et al. Assessment the exposure level of rare Earth elements in workers producing cerium, lanthanum oxide ultrafine and nanoparticles. *Biol. Trace Elem. Res.* **175** (2), 298–305 (2017).
5. Yuan, L. et al. La(2)O(3) nanoparticles induce reproductive toxicity mediated by the Nrf-2/ARE signaling pathway in Kunming mice. *Int. J. Nanomed.* **15**, 3415–3431 (2020).
6. Li, L. et al. Engineered nanodrug targeting oxidative stress for treatment of acute kidney injury. *Explor. (Beijing)*. **3** (6), 20220148 (2023).
7. Kermanizadeh, A. et al. An in vitro assessment of panel of engineered nanomaterials using a human renal cell line: cytotoxicity, pro-inflammatory response, oxidative stress and genotoxicity. *BMC Nephrol.* **14**, 96 (2013).
8. Hong, J. et al. Molecular mechanism of oxidative damage of lung in mice following exposure to lanthanum chloride. *Environ. Toxicol.* **30** (3), 357–365 (2015).
9. Li, R. et al. Interference in autophagosome fusion by rare Earth nanoparticles disrupts autophagic flux and regulation of an interleukin-1beta producing inflammasome. *ACS Nano*. **8** (10), 10280–10292 (2014).
10. Lu, V. M. et al. Cytotoxicity, dose-enhancement and radiosensitization of glioblastoma cells with rare Earth nanoparticles. *Artif. Cells Nanomed. Biotechnol.* **47** (1), 132–143 (2019).
11. Zhang, L. et al. Activation of Nrf2/ARE signaling pathway attenuates lanthanum chloride induced injuries in primary rat astrocytes. *Metallomics* **9** (8), 1120–1131 (2017).
12. Alyami, N. M. et al. Determination of dose- and time-dependent hepatotoxicity and apoptosis of lanthanum oxide nanoparticles in female Swiss albino mice. *Environ. Sci. Pollut Res. Int.* **31** (11), 17124–17139 (2024).
13. Doshi, S. M. & Wish, J. B. Past, present, and future of phosphate management. *Kidney Int. Rep.* **7** (4), 688–698 (2022).
14. Lacour, B. et al. Chronic renal failure is associated with increased tissue deposition of lanthanum after 28-day oral administration. *Kidney Int.* **67** (3), 1062–1069 (2005).
15. Nikolov, I. G. et al. Tissue accumulation of lanthanum as compared to aluminum in rats with chronic renal failure–possible harmful effects after long-term exposure. *Nephron Exp. Nephrol.* **115** (4), e112–e121 (2010).
16. Pratt, D. S. & Kaplan, M. M. Evaluation of abnormal liver-enzyme results in asymptomatic patients. *N Engl. J. Med.* **342** (17), 1266–1271 (2000).
17. Rao, X. et al. An improvement of the 2^(-delta delta CT) method for quantitative real-time polymerase chain reaction data analysis. *Biostat Bioinforma Biomath*. **3** (3), 71–85 (2013).
18. Yokoyama, T. et al. Identification of reference genes for quantitative PCR analyses in developing mouse gonads. *J. Vet. Med. Sci.* **80** (10), 1534–1539 (2018).
19. Bi, M. et al. Molecular mechanisms of lead-induced changes of selenium status in mice livers through interacting with Selenoprotein P. *Ecotoxicol. Environ. Saf.* **175**, 282–288 (2019).
20. Luo, M. et al. Tubeimoside I improves survival of mice in sepsis by inhibiting inducible nitric oxide synthase expression. *Biomed. Pharmacother.* **126**, 110083 (2020).
21. Brima, E. I. Determination of metal levels in Shamma (Smokeless Tobacco) with inductively coupled plasma mass spectrometry (ICP-MS) in najran, Saudi Arabia. *Asian Pac. J. Cancer Prev.* **17** (10), 4761–4767 (2016).
22. Kabir, H. et al. Influence of calcination on the sol–gel synthesis of lanthanum oxide nanoparticles. *Appl. Phys. A*. **124**, 1–11 (2018).
23. Wang, X. et al. A simple sol–gel technique for Preparing lanthanum oxide nanopowders. *Mater. Lett.* **60** (17–18), 2261–2265 (2006).
24. Salavati-Niasari, M., Hosseinzadeh, G. & Davar, F. Synthesis of lanthanum carbonate nanoparticles via sonochemical method for Preparation of lanthanum hydroxide and lanthanum oxide nanoparticles. *J. Alloys Compd.* **509** (1), 134–140 (2011).
25. Zhou, Q. et al. Nano La2O3 as a heterogeneous catalyst for biodiesel synthesis by transesterification of Jatropha curcas L. oil. *J. Ind. Eng. Chem.* **31**, 385–392 (2015).
26. Ismail, W. et al. Investigating the physical and electrical properties of La(2)O(3) via annealing of La(OH)(3). *Sci. Rep.* **14** (1), 7716 (2024).
27. Mossa, A. H., Swelam, E. S. & Mohafrash, S. M. M. Sub-chronic exposure to fipronil induced oxidative stress, biochemical and histopathological changes in the liver and kidney of male albino rats. *Toxicol. Rep.* **2**, 775–784 (2015).
28. Balusamy, B. et al. Toxicity of lanthanum oxide (La2O3) nanoparticles in aquatic environments. *Environ. Sci. Process. Impacts*. **17** (7), 1265–1270 (2015).
29. Li, Y. et al. *Direct quantification of rare Earth elements concentrations in urine of workers manufacturing cerium, lanthanum oxide ultrafine and nanoparticles by a developed and validated ICP-MS. Int. J. Environ. Res. Public. Health*, **13**(3). (2016).
30. Lu, N. H. et al. Examining the effects of dextran-based polymer-coated nanoparticles on amyloid fibrillogenesis of human insulin. *Colloids Surf. B Biointerfaces*. **172**, 674–683 (2018).
31. Lesniak, A. et al. Nanoparticle adhesion to the cell membrane and its effect on nanoparticle uptake efficiency. *J. Am. Chem. Soc.* **135** (4), 1438–1444 (2013).
32. Guo, Y. et al. Amphiphilic hybrid Dendritic-Linear molecules as nanocarriers for Shape-Dependent antitumor drug delivery. *Mol. Pharm.* **15** (7), 2665–2673 (2018).
33. D'Haese, P. C. et al. Lanthanum pharmacokinetics: are rat data misleading? *Kidney Int.* **68** (6), 2907–2908 (2005).
34. Nethi, S. K. et al. *Rare earth-based nanoparticles: biomedical applications, Pharmacological and toxicological significance. Nanopart. Their Biomedical Appl.*, : pp. 1–43. (2020).
35. Chen, M. et al. Systematic oxidative stress is not associated with live birth rate in young non-obese patients with polycystic ovarian syndrome undergoing assisted reproduction cycles: A prospective cohort study. *Eur. J. Obstet. Gynecol. Reprod. Biol.* **253**, 154–161 (2020).
36. Dressler, V. L. et al. Investigative analysis of lanthanum oxide nanoparticles on elements in bone of Wistar rats after 30 days of repeated oral administration. *Biol. Trace Elem. Res.* **196** (1), 153–167 (2020).
37. Huang, K. et al. Comparison of toxicity between lanthanum oxide nanoparticles and lanthanum chloride. *J. Rare Earths*. **42** (2), 424–430 (2024).

38. Kar, F. et al. The role of oxidative stress, renal inflammation, and apoptosis in post ischemic reperfusion injury of kidney tissue: the protective effect of Dose-Dependent boric acid administration. *Biol. Trace Elem. Res.* **195** (1), 150–158 (2020).
39. Navaratnarajah, A. et al. Systemic inflammation and oxidative stress contribute to acute kidney injury after transcatheter aortic valve implantation. *Cardiol. J.* **29** (5), 824–835 (2022).
40. Al-Sultany, H. H. A. et al. Cardamonin mitigates kidney injury by modulating inflammation, oxidative stress, and apoptotic signaling in rats subjected to renal ischemia and reperfusion. *J. Med. Life*. **16** (12), 1852–1856 (2023).
41. Zima, T. et al. Lipid peroxidation and antioxidant enzymes in CAPD patients. *Ren. Fail.* **18** (1), 113–119 (1996).
42. Mimić-Oka, J. et al. Alteration in plasma antioxidant capacity in various degrees of chronic renal failure. *Clin. Nephrol.* **51** (4), 233–241 (1999).
43. Kirkman, H. N. et al. Mechanisms of protection of catalase by NADPH: kinetics and stoichiometry. *J. Biol. Chem.* **274** (20), 13908–13914 (1999).
44. Yilmaz, M. I. et al. The determinants of endothelial dysfunction in CKD: oxidative stress and asymmetric dimethylarginine. *Am. J. Kidney Dis.* **47** (1), 42–50 (2006).
45. Vodošek Hojs, N. et al. Oxidative stress markers in chronic kidney disease with emphasis on diabetic nephropathy. *Antioxidants* **9** (10), 925 (2020).
46. Li, S. Q. et al. Nanotoxicity of TiO(2) nanoparticles to erythrocyte in vitro. *Food Chem. Toxicol.* **46** (12), 3626–3631 (2008).
47. Shang, L., Nienhaus, K. & Nienhaus, G. U. Engineered nanoparticles interacting with cells: size matters. *J. Nanobiotechnol.* **12**, 5 (2014).
48. Almukhlafi, H. et al. Role of oxidative stress in La(2)O(3) Nanoparticle-Induced cytotoxicity and apoptosis in CHANG and HuH-7 cells. *Int. J. Nanomed.* **16**, 3487–3496 (2021).
49. Lu, V. M., Jue, T. R. & McDonald, K. L. Cytotoxic lanthanum oxide nanoparticles sensitize glioblastoma cells to radiation therapy and temozolomide: an in vitro rationale for translational studies. *Sci. Rep.* **10** (1), 18156 (2020).
50. Yuan, L. et al. Effects of intragastric administration of La2O3 nanoparticles on mouse testes. *J. Toxicol. Sci.* **45** (8), 411–422 (2020).
51. Ookhtens, M. & Kaplowitz, N. Role of the liver in interorgan homeostasis of glutathione and cyst(e)ine. *Semin Liver Dis.* **18** (4), 313–329 (1998).
52. Fadia, B. S. et al. Histological injury to rat brain, liver, and kidneys by gold nanoparticles is Dose-Dependent. *ACS Omega*. **7** (24), 20656–20665 (2022).
53. Noor, K. K. et al. Hepatoprotective role of vitexin against cadmium-induced liver damage in male rats: A biochemical, inflammatory, apoptotic and histopathological investigation. *Biomed. Pharmacother*. **150**, 112934 (2022).
54. Sharifi-Rad, M. et al. Lifestyle, oxidative stress, and antioxidants: back and forth in the pathophysiology of chronic diseases. *Front. Physiol.* **11**, 694 (2020).
55. Grebowski, R. et al. The role of SOD2 and NOS2 genes in the molecular aspect of bladder cancer pathophysiology. *Sci. Rep.* **13** (1), 14491 (2023).
56. Udi, S. et al. Dual Inhibition of cannabinoid CB(1) receptor and inducible NOS attenuates obesity-induced chronic kidney disease. *Br. J. Pharmacol.* **177** (1), 110–127 (2020).
57. Abdel-Rahman, D. M. et al. Regulation of renal nitric oxide and eNOS/iNOS expression by Tadalafil participates in the mitigation of amphotericin B-induced renal injury: Down-regulation of NF-kappaB/iNOS/caspase-3 signaling. *Naunyn Schmiedebergs Arch. Pharmacol.* **397** (5), 3141–3153 (2024).
58. Bhosale, S. J. & Kulkarni, A. P. Biomarkers in acute kidney injury. *Indian J. Crit. Care Med.* **24** (Suppl 3), S90–S93 (2020).
59. Aboelwafa, H. R. et al. *Modulation effects of Eugenol on nephrotoxicity triggered by silver nanoparticles in adult rats*. *Biology (Basel)*, (2022). 11(12).
60. Elkhateeb, S. A. et al. Ameliorative role of Curcumin on copper oxide nanoparticles-mediated renal toxicity in rats: an investigation of molecular mechanisms. *J. Biochem. Mol. Toxicol.* **34** (12), e22593 (2020).
61. Srivastava, A. et al. Uric acid and acute kidney injury in the critically ill. *Kidney Med.* **1** (1), 21–30 (2019).
62. Chavez-Iniguez, J. S. et al. Urea reduction in acute kidney injury and mortality risk. *Kidney Blood Press. Res.* **48** (1), 357–366 (2023).
63. Kan, L. et al. Rho-Associated kinase inhibitor (Y-27632) attenuates Doxorubicin-Induced apoptosis of human cardiac stem cells. *PLoS One*. **10** (12), e0144513 (2015).
64. Zhu, Y. et al. IGF2 deficiency causes mitochondrial defects in skeletal muscle. *Clin. Sci. (Lond)*. **135** (7), 979–990 (2021).
65. Zhang, C. et al. NTRK1-mediated protection against manganese-induced neurotoxicity and cell apoptosis via IGF2 in SH-SY5Y cells. *Biomed. Pharmacother*. **169**, 115889 (2023).
66. Bach, L. A. & Hale, L. J. Insulin-like growth factors and kidney disease. *Am. J. Kidney Dis.* **65** (2), 327–336 (2015).
67. Sisler, J. D. et al. Differential pulmonary effects of CoO and La2O3 metal oxide nanoparticle responses during aerosolized inhalation in mice. *Part. Fibre Toxicol.* **13** (1), 42 (2016).
68. Cuarental, L. et al. The transcription factor Fosl1 preserves Klotho expression and protects from acute kidney injury. *Kidney Int.* **103** (4), 686–701 (2023).
69. Kirita, Y. et al. Cell profiling of mouse acute kidney injury reveals conserved cellular responses to injury. *Proc. Natl. Acad. Sci. U S A*. **117** (27), 15874–15883 (2020).
70. Justo, P. et al. *Expression of smac/diablo in tubular epithelial cells and during acute renal failure*. *Kidney Int. Suppl.*, **2003**(86): pp. S52–S56 .
71. Tabara, L. C. et al. Mitochondria-targeted therapies for acute kidney injury. *Expert Rev. Mol. Med.* **16**, e13 (2014).
72. Wang, L., Du, F. & Wang, X. TNF-alpha induces two distinct caspase-8 activation pathways. *Cell* **133** (4), 693–703 (2008).
73. Tang, C. et al. P53 in kidney injury and repair: mechanism and therapeutic potentials. *Pharmacol. Ther.* **195**, 5–12 (2019).
74. Al-Lamki, R. S. & Mayadas, T. N. TNF receptors: signaling pathways and contribution to renal dysfunction. *Kidney Int.* **87** (2), 281–296 (2015).
75. Lorz, C. et al. The death ligand TRAIL in diabetic nephropathy. *J. Am. Soc. Nephrol.* **19** (5), 904–914 (2008).
76. Bernardi, S. et al. TRAIL, OPG, and TWEAK in kidney disease: biomarkers or therapeutic targets? *Clin. Sci. (Lond)*. **133** (10), 1145–1166 (2019).
77. O'Neill, S. et al. Heat-shock proteins and acute ischaemic kidney injury. *Nephron Exp. Nephrol.* **126** (4), 167–174 (2014).
78. Kim, M. et al. Selective renal overexpression of human heat shock protein 27 reduces renal ischemia-reperfusion injury in mice. *Am. J. Physiol. Ren. Physiol.* **299** (2), F347–F358 (2010).
79. Sonoda, H. et al. The protective effect of radicicol against renal ischemia–reperfusion injury in mice. *J. Pharmacol. Sci.* **112** (2), 242–246 (2010).
80. Chiang, M. C. et al. Nanogold induces anti-inflammation against oxidative stress induced in human neural stem cells exposed to amyloid-beta peptide. *Neurochem Int.* **145**, 104992 (2021).
81. Liao, M. & Liu, H. Gene expression profiling of nephrotoxicity from copper nanoparticles in rats after repeated oral administration. *Environ. Toxicol. Pharmacol.* **34** (1), 67–80 (2012).
82. Özgür, A. et al. Green synthesis of silver nanoparticles using macrolepiota procera extract and investigation of their HSP27, HSP70, and HSP90 inhibitory potentials in human cancer cells. *Part. Sci. Technol.* **41** (3), 330–340 (2023).
83. He, K. et al. Hsp90 inhibitors promote p53-dependent apoptosis through PUMA and Bax. *Mol. Cancer Ther.* **12** (11), 2559–2568 (2013).

84. Özgür, A. Investigation of anticancer activities of STA-9090 (ganetespib) as a second generation HSP90 inhibitor in Saos-2 osteosarcoma cells. *J. Chemother.* **33** (8), 554–563 (2021).
85. Aghadavod, E. et al. Comparison between biomarkers of kidney injury, inflammation, and oxidative stress in patients with diabetic nephropathy and type 2 diabetes mellitus. *Iran. J. Kidney Dis.* **14** (1), 31–35 (2020).
86. Smaili, S. S. et al. The role of calcium stores in apoptosis and autophagy. *Curr. Mol. Med.* **13** (2), 252–265 (2013).
87. Wang, Y. et al. The protective effects of selenium on cadmium-induced oxidative stress and apoptosis via mitochondria pathway in mice kidney. *Food Chem. Toxicol.* **58**, 61–67 (2013).
88. El-Boshy, M. et al. Vitamin D(3) and calcium cosupplementation alleviates cadmium hepatotoxicity in the rat: enhanced antioxidative and anti-inflammatory actions by remodeling cellular calcium pathways. *J. Biochem. Mol. Toxicol.* **34** (3), e22440 (2020).
89. Reeves, P. G. & Chaney, R. L. Marginal nutritional status of zinc, iron, and calcium increases cadmium retention in the duodenum and other organs of rats fed rice-based diets. *Environ. Res.* **96** (3), 311–322 (2004).
90. Reeves, J. P. & Condrescu, M. Lanthanum is transported by the sodium/calcium exchanger and regulates its activity. *Am. J. Physiol. Cell. Physiol.* **285** (4), C763–C770 (2003).
91. Lingamdinne, L. P. et al. Stable and recyclable lanthanum hydroxide-doped graphene oxide biopolymer foam for superior aqueous arsenate removal: insight mechanisms, batch, and column studies. *Chemosphere* **313**, 137615 (2023).
92. Rezania, S. et al. Removal of lead ions from wastewater using lanthanum sulfide nanoparticle decorated over magnetic graphene oxide. *Environ. Res.* **204(Pt A)**, p111959 (2022).
93. Gerber, L. C. et al. Phosphate starvation as an antimicrobial strategy: the controllable toxicity of lanthanum oxide nanoparticles. *Chem. Commun. (Camb).* **48** (32), 3869–3871 (2012).
94. Zhang, L. et al. Removal of phosphate from water by activated carbon fiber loaded with lanthanum oxide. *J. Hazard. Mater.* **190** (1–3), 848–855 (2011).

Acknowledgements

We thank Dr. Daoud Ali, Dr. Doaa M. Elnagar, and Dr. Ahmed Rady for providing materials and chemicals, and Dr. Norah S. Alothman for helping during the animal dissection.

Author contributions

N.A, G.A, R.A, and Saud. A conceptualized the study; N.A, H.M.A, and H.A were responsible for the data curation; N. A. and G. A. were responsible for the formal analysis; NA was accountable for the funding acquisition; N.M. A, N.A, S.M, K.F, Z.N, F.A, S.AQ, and G.A were accountable for the investigation, N. A and G.A were responsible for the methodology; S.A and R.A were accountable for the project administration; G.A and S.M were responsible for the software; N.A supervised the study; RA was responsible for the validation; G.A and N.A wrote the original draft and N.A reviewed and edited the manuscript.

Funding

The authors extend their appreciation to the Deputyship for Research & Innovation, "Ministry of Education" in Saudi Arabia, for funding this research work through the project number (IFKSUDR_H231).

Ethics declarations

Competing interests

The authors declare no competing interests.

Ethics approval

The experimental protocol was approved by King Saud University's Institutional Animal Care and Use Committee (IACUC) (Ref. No.: KSU-SE-22-75).

Additional information

Supplementary Information The online version contains supplementary material available at https://doi.org/10.1038/s41598-025-04996-0.

Correspondence and requests for materials should be addressed to N.M.A.